

High Temperature Corrosion and Characterization Studies in Flux Cored Arc Welded 2.25Cr-1Mo Power Plant Steel

S.P. Kumaresh Babu and S. Natarajan

(Submitted April 18, 2006; in revised form July 2, 2009)

Higher productivity is registered with Flux cored arc welding (FCAW) process in many applications. Further, it combines the characteristics of shielded metal arc welding (SMAW), gas metal arc welding (GMAW), and submerged arc welding (SAW) processes. This article describes the experimental work carried out to evaluate and compare corrosion and its inhibition in SA 387 Gr.22 (2.25Cr-1Mo) steel weldments prepared by FCAW process with four different heat inputs exposed to hydrochloric acid medium at 0.1, 0.5, and 1.0 M concentrations. The parent metal, weld metal, and heat-affected zone are chosen as regions of exposure for the study carried out at 100 °C. Electrochemical polarization techniques such as Tafel line extrapolation (Tafel) and linear polarization resistance (LPR) have been used to measure the corrosion current. The role of hexamine and mixed inhibitor (thiourea + hexamine in 0.5 M HCl), each at 100 ppm concentration is studied in these experiments. Microstructural observation, hardness survey, surface characterization, and morphology using scanning electron microscope (SEM) and x-ray diffraction (XRD) have been made on samples to highlight the nature and extent of film formation. The film is found to contain Fe_2Si , FeSi_2 , FeMn_3 , Fe_7Mo_3 , Fe_3O_4 , FeO , FeCr , $\text{AlO}_7\text{Fe}_3\text{SiO}_3$, and $\text{KFe}_4\text{Mn}_{77}\text{Si}_{19}$.

Keywords FCAW, heat input, hexamine, high temperature corrosion, microstructure, power plant 2.25Cr-1Mo steel, SEM, XRD

1. Aim and Scope

FCAW is a better alternative to SMAW, and its extensive use is due to inherent process and metallurgical advantages (Ref 1, 2) such as: (i) high-quality weld metal (WM) deposit, (ii) excellent weld bead appearance, (iii) higher deposition rate (four times more than SMAW), (iv) reduced distortion, and (v) higher tolerance for contaminants that may cause weld cracking, and (vi) resistance to under bead cracking. In addition to these, a faster burn off rate for tubular FCAW is promoted by higher current densities at the wire tip. Also the duty cycle obtainable with the FCAW process is higher than GTAW and SMAW. The higher duty cycle can be attributed to two main factors: the continuous nature of the process and all-positional capability of the process without the need for a change in the welding parameters. In all the arc welding processes (Ref 3, 4), intense heat source produced by the arc and the associated local heating and cooling result in a number of consequences in material corrosion behavior, and several metallurgical phase changes occur in different zones of a weldment. Because corrosion phenomenon is due to occurrence of electrochemical potential gradient in the adjacent sites of a WM, it is proposed to study the effects of welding on the corrosion behavior of

these steels. The fossil fuel-fired boilers (Ref 5-7) and power generating equipment experience corrosion problems in such components as steam generators, water walls surrounding the furnace, and in the front and rear portions of the superheater and reheater. These components are often made of carbon and Cr-Mo steels. The water used for raising steam in any boiler installation often contains gaseous impurities and dissolved solids. These can cause scaling and corrosion in the boiler plant. Apart from these, some of the inorganic salts hydrolyze to produce acidity causing corrosion of boiler tubes.

This article describes an experimental work carried out at 100 °C to evaluate and compare corrosion, and its inhibition of SA 387 Gr.22 (2.25Cr-1Mo) steel weldments prepared by FCAW process with four different heat inputs in HCl acid medium. Organic compounds such as hexamine and thiourea were used as inhibitors for the prevention of corrosion. In this study, hexamine, thiourea, and mixture of these two each at 100 ppm concentration was individually employed as inhibitor. SEM and XRD analyses were also made on samples.

2. Experimental Work

2.1 Preparation of Weldments

2.25Cr-1Mo steel in plate form was welded by FCAW process with four different heat inputs, and it was stress relieved at 720 °C. The studies were made using small coupons measuring 90 mm (width) × 10 mm (thickness) cut from the plate comprising parent metal (PM) and WM regions. The plate had original dimensions of 300 mm (length) × 150 mm (width) × 10 mm (thick). Two such plates were taken with a V groove and welded. The test coupons were cut from the plate in transverse direction. These specimens only were utilized for experimentation purpose.

S.P. Kumaresh Babu and S. Natarajan, Department of Metallurgical & Materials Engineering, National Institute of Technology, Tiruchirappalli 620 015, Tamilnadu, India. Contact e-mails: kumaresh1965@yahoo.co.in and drs_natarajan@yahoo.com.

2.2 Corrosive Medium and Inhibitor

HCl acid solutions of 0.1, 0.5, and 1.0 M concentrations were prepared using analar grade materials. Hexamine at 100 ppm was used as the inhibitor throughout the study. The role of mixed inhibitor (thiourea + hexamine in 0.5 M HCl) each at 100 ppm concentration was also studied. Each test coupon was surface polished using conventional methods (degreasing, polishing with emery papers of various grades, etc.). Except the desired area of region of exposure, the other regions were masked using Teflon. Study was carried out at 100 °C. The heat-affected zone (HAZ) was identified by macroetching.

2.3 Electrochemical Polarization Studies

All studies were made using Model-362 scanning potentiostat (Princeton Applied Research Corp., USA). The study was made at 100 °C and was undertaken in both cathodic and anodic regions in the absence and presence of inhibitor mentioned above. The following techniques were adopted to find I_{corr} values.

2.4 Tafel Line Exploration

Applications of potential up to ± 150 mV from open circuit potential (OCP) were made for Tafel method, and a plot of E versus $\log i$ was made in all the experiments and tangents were drawn, which on extrapolation to E_{corr} , intersected at a point that is represented on the X axis, as the I_{corr} value.

2.5 Linear Polarization Resistance (LPR)

The OCP in each case was observed after the system became stable at least for 30 min. Accordingly, the OCP upto 20 mV potentials were applied in a discrete fashion in increments of 2 mV, and corresponding current was read. A plot of E versus I was made. It was found to be linear almost in all the cases. From the above plot, R_p was calculated. I_{corr} values were obtained using the formula

$$I_{\text{corr}} = b_a b_c / 2.303(b_a + b_c) \cdot 1/R_p$$

where $R_p = \Delta E/\Delta I$, b_a , and b_c values were obtained from the Tafel line extrapolation method as described above.

Table 1 Chemical composition in wt.% and mechanical properties for SA 387 Gr.22 steel

Element:	C	Mn	Si	P	S	Mo	Cr	T.S, MPa	Y.S, MPa
Base metal	0.15 max	0.3-0.6	0.5-1.0	0.03 max	0.03 max	0.90-1.20	2.0-2.5	415.0	205.0
Filler wire AWS-E90-T5 B ₃	0.10	1.41	0.47	0.017	0.010	1.0	2.25	480.0	400.0

Table 2 Chemical analysis of weld metal and base metal

Sample ID	C	Mn	Si	S	P	Cr	Ni	Mo	V	Cu
PM	0.13	0.46	0.26	<0.010	<0.010	2.40	<0.10	0.89	<0.05	<0.10
H.I-1WM	0.09	1.54	0.53	<0.010	<0.010	2.59	<0.10	1.22	<0.05	<0.10
H.I-2WM	0.09	1.32	0.53	<0.010	<0.010	2.60	<0.10	1.19	<0.05	<0.10
H.I-3WM	0.08	1.22	0.45	<0.010	<0.011	2.17	<0.10	0.91	<0.05	<0.10
H.I-4WM	0.08	1.30	0.47	<0.010	<0.012	2.35	<0.10	0.96	<0.05	<0.10

2.6 SEM Analysis

Studies on the surface morphologies of 2.25Cr-1Mo samples were carried out for the weld root region exposed to 0.5 M concentration at 100 °C containing the hexamine inhibitor at 100 ppm level using scanning electron microscope (JEOL make, Japan).

2.7 XRD Studies

A computer-controlled wide angle x-ray diffractometer system JEOL model; JDX 8030 using Cu K α radiation and $\lambda = 1.5418 \text{ \AA}$ (Ni filter) with a scanning range 3-65° 2 θ was used to investigate the weld region of the specimen.

2.8 Chemical Composition

The data related to chemical composition and mechanical properties for SA 387 Gr.22 steel (base metal) and Filler wire AWS-E90-T5 B₃ were referred and utilized from ASME standards. The chemical compositions of respective WMs (mentioned in Table 2) and that of base metal (i.e., parent metal:PM) for comparison purpose were obtained using optical emission spectrometer (Hilger Analytical Make, Polyvac 2000, UK).

3. Results and Discussion

The chemical composition and mechanical properties, typical WM chemical analyses, and welding conditions for the SA 387 Gr.22 (2.25Cr-1Mo) steel are given in Table 1-3.

3.1 Selection of Electrochemical Technique

The I_{corr} values obtained through Tafel and LPR techniques for Parent Metal (PM), Weld Metal (WM) and HAZ regions with different heat inputs are given in Table 4-6. The corrosion currents for both Tafel and LPR technique are higher for WM than HAZ and PM regions. The maximum inhibitor efficiency observed is 93.0% in HAZ region.

3.2 Effect of Acid Concentration

The corrosion rate increases with increase in acid concentration for all the regions with few exceptions in HAZ.

Table 3 Welding parameters for FCAW process with four different heat inputs

Parameters	Current, A	Voltage, V	Gas flow rate, L/min	Shielding gas	Heat input, J/mm
Heat input 1	160	24	20	80%Ar + 20%CO ₂	1152
Heat input 2	160	24	20	80%Ar + 20%CO ₂	1612
Heat input 3	220	24	20	80%Ar + 20%CO ₂	2112
Heat input 4	220	24	20	80%Ar + 20%CO ₂	2640

Table 4 I_{corr} in mA/cm² for 2.25Cr-1Mo/FCAW/HCl/PM/hexamine/100 °C

Heat input:			Tafel	LPR
Concentration	0.1 M	WoI	0.45	0.15
		WI	0.38 (15.5)	0.41 (IAC)
	0.5 M	WoI	0.70	0.38
		WI	0.60 (14.2)	0.45 (IAC)
	1.0 M	WoI	0.49	0.70
		WI	0.38 (22.0)	0.30 (57.1)

Note: H.I, heat input; WoI, without inhibitor; PIE, percentage inhibitor efficiency; WI, with inhibitor; (), PIE for FCAW process; IAC, inhibitor accelerates corrosion

3.3 Influence of Heat Input, Welding Process, Hardness, and Microstructure

The microstructure of HAZ, WM, and PM are shown in Fig. 1-9, and the hardness survey plot and hardness impression micrograph are shown in Fig. 10 and 11. It is observed that at 100 °C, with increasing heat input, corrosion rate increases for WM region and HAZ regions. The following reason may be attributed to this observation: The weldmetal microstructure consists of acicular ferrite, tempered and untempered martensite, and alloy carbides whereas in the HAZ region, widmanstatten ferrite, pearlite, and martensite are observed. In two-phase alloys, two phases may form a galvanic couple at the micro structural level, and electrical contact between them is inherent in the structure. The tempered martensite present in the WM

Table 5 I_{corr} in mA/cm² for 2.25Cr-1Mo/FCAW/HCl/WM/hexamine/100 °C

Different heats input:			H.I 1	H.I 2	H.I 3	H.I 4
Tafel	0.1 M	WoI	1.30	2.3	1.0	2.6
		WI	0.54 (58.4)	2.9 (IAC)	1.3 (IAC)	1.6 (38.4)
	0.5 M	WoI	1.2	2.7	0.92	3.8
		WI	0.9 (25.0)	2.5 (7.4)	1.1 (IAC)	3.5 (7.8)
	1.0 M	WoI	5.0	2.6	2.0	8.0
		WI	6.0 (IAC)	18.0 (IAC)	4.0 (IAC)	8.1 (IAC)
LPR	0.1 M	WoI	1.72	1.93	0.54	4.44
		WI	0.26 (84.8)	5.14 (IAC)	1.25 (IAC)	2.97 (33.1)
	0.5 M	WoI	0.53	3.52	0.64	2.67
		WI	0.30 (43.3)	1.16 (67.0)	0.52 (18.7)	3.37 (IAC)
	1.0 M	WoI	1.16	1.97	0.6	2.15
		WI	3.83 (IAC)	12.39 (IAC)	1.25 (IAC)	5.81 (IAC)

Table 6 I_{corr} in mA/cm² for 2.25Cr-1Mo/FCAW/HCl/HAZ/hexamine/100 °C

Different heats input:			H.I 1	H.I 2	H.I 3	H.I 4
Tafel	0.1 M	WoI	0.6	1.2	1.6	2.1
		WI	0.88 (IAC)	1.21 (IAC)	1.8 (IAC)	2.4 (IAC)
	0.5 M	WoI	2.0	1.2	1.8	3.4
		WI	0.98 (51.0)	0.46 (61.6)	2.3 (IAC)	3.41 (IAC)
	1.0 M	WoI	0.8	1.6	1.4	6.0
		WI	1.0 (IAC)	7.0 (IAC)	1.6 (IAC)	10.0 (IAC)
LPR	0.1 M	WoI	0.59	1.85	1.92	2.87
		WI	0.54 (8.4)	1.74 (5.9)	2.56 (IAC)	1.93 (32.7)
	0.5 M	WoI	1.0	0.86	0.42	2.0
		WI	0.43 (57.0)	2.28 (IAC)	1.08 (IAC)	5.59 (IAC)
	1.0 M	WoI	0.50	0.93	0.47	3.73
		WI	0.82 (IAC)	0.28 (69.8)	0.65 (IAC)	0.26 (93.0)

Note: H.I, heat input; WoI, without inhibitor; PIE, percentage inhibitor efficiency; WI, with inhibitor; (), PIE for FCAW process; IAC, inhibitor accelerates corrosion

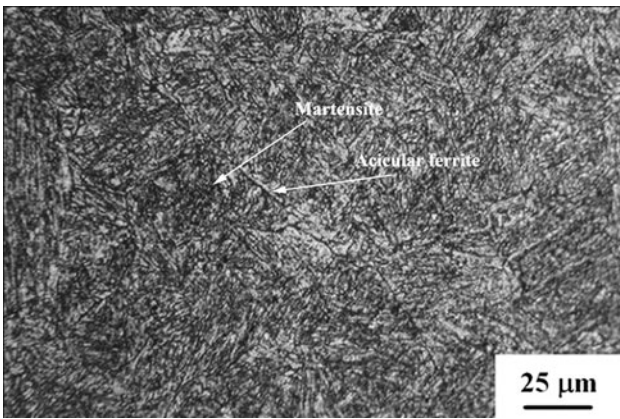


Fig. 1 Microstructure of HAZ/SA387Gr22/FCAW with heat input 1 (1152 J/mm) consisting of acicular ferrite and martensite

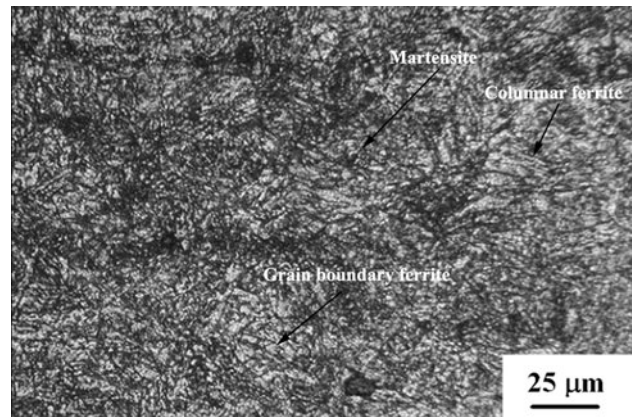


Fig. 4 Microstructure of HAZ/SA387Gr22/FCAW with heat input 4 (2640 J/mm) consisting of grain boundary ferrite, columnar ferrite, and martensite

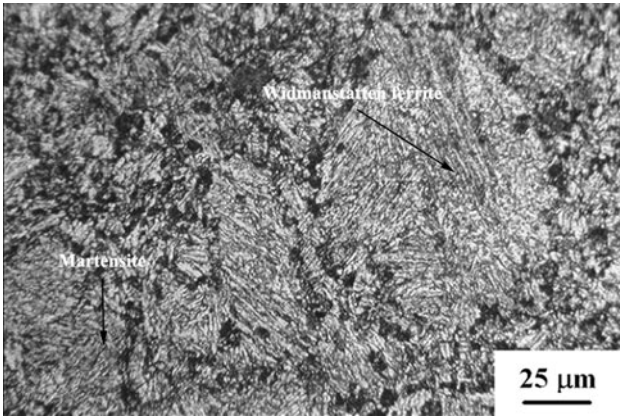


Fig. 2 Microstructure of HAZ/SA387Gr22/FCAW with heat input 2 (1612 J/mm) consisting of widmanstätten ferrite and martensite

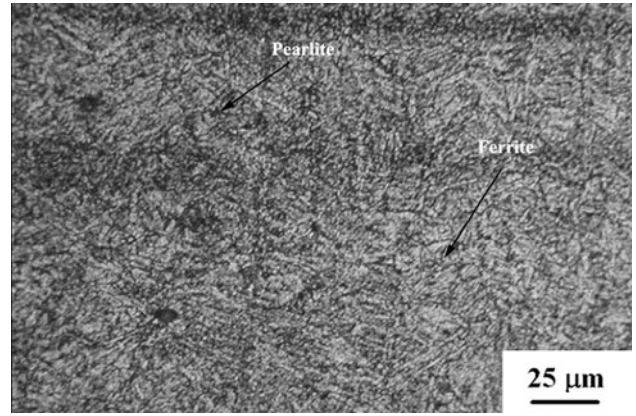


Fig. 5 Microstructure of PM. Structure consists of fine ferrite and pearlite

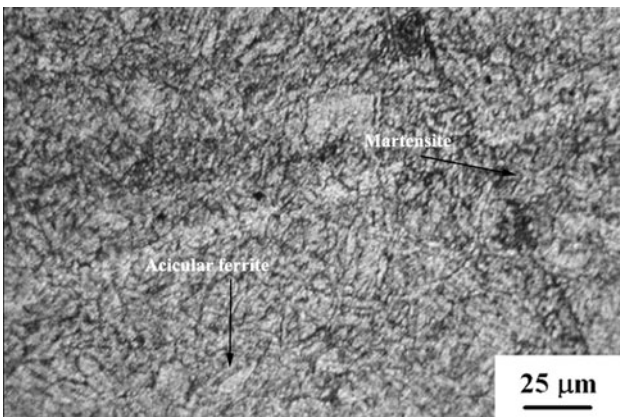


Fig. 3 Microstructure of HAZ/SA387Gr22/FCAW with heat input 3 (2112 J/mm) consisting of acicular ferrite, bainite, and martensite

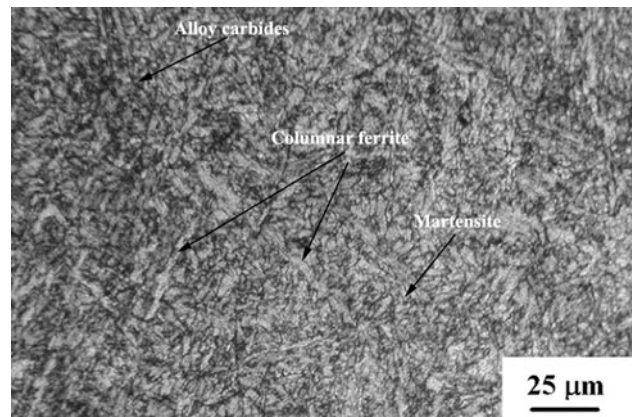


Fig. 6 Microstructure of WM/SA387Gr22/FCAW with heat input 1 (1152 J/mm) consisting of columnar ferrite, martensite, and alloy carbides

becomes anodic to untempered martensite and carbides, and leads to higher corrosion damage. It is seen that employment of higher temperature has accelerated corrosion in all the regions at all acidic concentrations which can be because of increase in mobility of the ions due to higher diffusion and higher activation energy at the grain boundaries (Ref 8).

From the hardness, it is inferred that WM shows higher hardness in all the heat inputs. This is due to the presence of carbides, and it is indicated through the projection/profile of hardness impression also. The hardness and weld chemistry do change the corrosion scenario under test conditions.

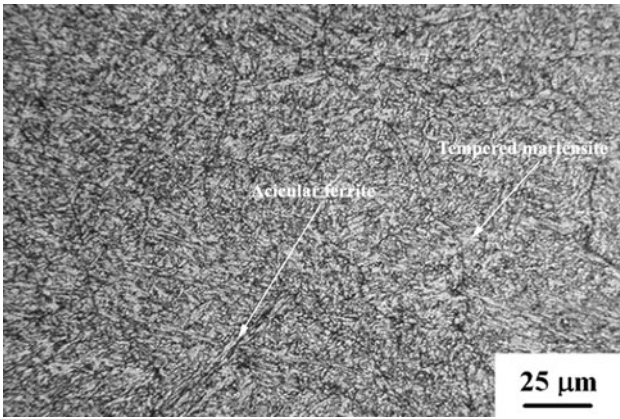


Fig. 7 Microstructure of WM/SA387Gr22/FCAW with heat input 2 (1612 J/mm) consisting of acicular ferrite and tempered martensite

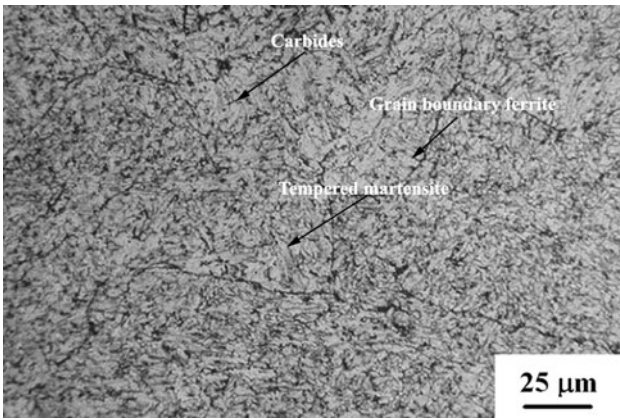


Fig. 8 Microstructure of WM/SA387Gr22/FCAW with heat input 3 (2112 J/mm) consisting of grain boundary ferrite, carbides, and tempered martensite

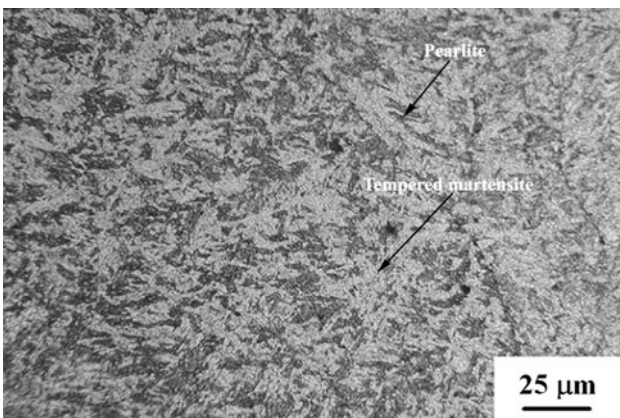


Fig. 9 Microstructure of WM/SA387Gr22/FCAW with heat input 4 (2640 J/mm) consisting of carbides, pearlite, and tempered martensite

3.4 Role of Inhibitor

Hexamine: It is the weld root region which always carries the corrosive fluids during the operation of any plant. Hexamine shows 84.8% efficiency at 100 °C for WM region

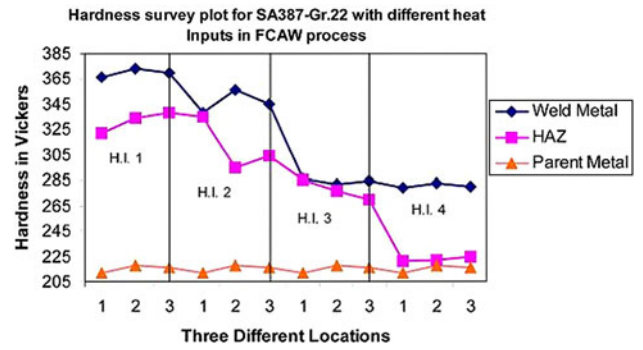


Fig. 10 Hardness survey plot for SA 387 Gr.22 with different heat inputs in FCAW process

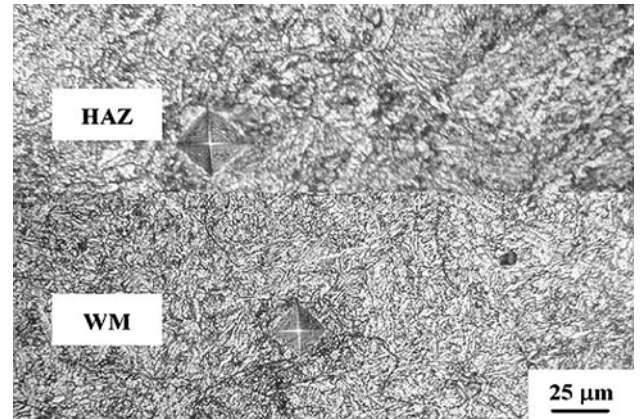


Fig. 11 Impressions of hardness indentations on WM and HAZ for 2.25Cr-1Mo steel

in LPR technique. An important observation is that more than 90% of the experiments performed with this inhibitor are found to accelerate the corrosion phenomenon. Hence, it can be said that the use of hexamine at high temperature is not suitable for 2.25Cr-1Mo material though hexamine is the best known for inhibiting acidic corrosion only for plain carbon steels. In other words, the percentages of inhibitor efficiencies are poor in the case of FCAW process at 100 °C when compared to those at room temperature studies made with the same material (Ref 9). This was due to the reason that the greatest coverage density on the metallic surface by the inhibitor can be obtained with saturated long-chain compounds rather than with those having branched chains, because of their lateral orientations. Again, because of their spatial arrangement, the chains of tertiary amines give a smaller coverage and therefore a lower degree of inhibition (Ref 10). From an earlier study and a comparison from reports of case studies, it is confirmed that use of hexamine and mixed inhibitor is not beneficial to 2.25Cr-1Mo/FCAW weldments at 100 °C (Ref 11).

Thiourea: The I_{corr} values for WM and HAZ are given in Table 7 and 8. For HAZ region 33.0% efficiency is shown by thiourea at 100 °C.

Mixed inhibitor (thiourea + hexamine): The I_{corr} values for WM and HAZ are given in Table 7 and 8. For the WM region mixed inhibitor shows a maximum of 50.0% whereas in HAZ it shows 47% efficiency at 100 °C. A comparison of P.I.E. values for 0.5 M HCl with different inhibitors with varied heat inputs

Table 7 I_{corr} in mA/cm² for 2.25Cr-1Mo/FCAW/0.5 M HCl/WM/thiourea/mixed inhibitor/100 °C

Different heats input:			H.I 1	H.I 2	H.I 3	H.I 4
Tafel	0.5 M	WoI	1.2	2.7	0.92	3.8
		WI (thio)	4.6 (IAC)	7.4 (IAC)	1.5 (IAC)	4.0 (IAC)
		WI (mixed)	6.0 (IAC)	6.8 (IAC)	2.5 (IAC)	2.4 (50.0)
LPR	0.5 M	WoI	0.53	5.14	0.64	2.67
		WI (thio)	6.15 (IAC)	5.76 (IAC)	1.13 (IAC)	4.34 (IAC)
		WI (mixed)	7.26 (IAC)	2.69 (47.6)	3.12 (IAC)	5.77 (IAC)

Table 8 I_{corr} in mA/cm² for 2.25Cr-1Mo/FCAW/0.5 M HCl/HAZ/thiourea/mixed inhibitor/100 °C

Different heats input:			H.I 1	H.I 2	H.I 3	H.I 4
Tafel	0.5 M	WoI	2.0	1.2	1.8	3.4
		WI (thio)	1.35 (32.5)	6.0 (IAC)	5.0 (IAC)	2.8 (17.6)
		WI (mixed)	1.1 (45.0)	5.8 (IAC)	1.4 (22.2)	7.8 (IAC)
LPR	0.5 M	WoI	1.0	0.86	0.42	2.0
		WI (thio)	0.77 (33.0)	2.58 (IAC)	3.59 (IAC)	2.75 (IAC)
		WI (mixed)	0.53 (47.0)	5.76 (IAC)	0.86 (IAC)	5.6 (IAC)

Table 9 Comparison of PIE for 2.25Cr-1Mo/FCAW/0.5 M HCl/WM/hexamine/thiourea/mixed inhibitor/100 °C

Different heats input:			H.I 1	H.I 2	H.I 3	H.I 4
Tafel	0.1 M	Hexa.	58.4	IAC	IAC	38.4
		Thio.	IAC	IAC	IAC	IAC
	0.5 M	Hexa.	25.0	7.4	IAC	7.8
		Mixed	IAC	IAC	IAC	50.0
LPR	1.0 M	Hexa.	IAC	IAC	IAC	IAC
		Mixed	IAC	IAC	IAC	IAC
	0.1 M	Hexa.	84.8	IAC	IAC	33.1
		Mixed	IAC	IAC	IAC	IAC
0.5 M	Hexa.	43.3	67.0	18.7	IAC	
	Thio.	IAC	IAC	IAC	IAC	
	Mixed	IAC	47.6	IAC	IAC	
	Hexa.	IAC	IAC	IAC	IAC	

Note: H.I, heat input; WoI, without inhibitor; PIE, percentage inhibitor efficiency; WI, with inhibitor; (), PIE for FCAW process; IAC, inhibitor accelerates corrosion

Table 10 Comparison of PIE for 2.25Cr-1Mo/FCAW/0.5 M HCl/HAZ/hexamine/thiourea/mixed inhibitor/100 °C

Different heats input:			H.I 1	H.I 2	H.I 3	H.I 4
Tafel	0.1 M	Hexa.	IAC	IAC	IAC	IAC
		Thio.	32.5	IAC	IAC	17.6
	0.5 M	Hexa.	51.0	61.6	IAC	IAC
		Mixed	45.0	IAC	22.2	IAC
LPR	1.0 M	Hexa.	IAC	IAC	IAC	IAC
		Mixed	IAC	IAC	IAC	IAC
	0.1 M	Hexa.	8.4	5.9	IAC	32.7
		Mixed	IAC	IAC	IAC	IAC
0.5 M	Hexa.	57.0	IAC	IAC	IAC	
	Thio.	33.0	IAC	IAC	IAC	
	Mixed	47.0	IAC	IAC	IAC	
	Hexa.	IAC	69.8	IAC	93.0	

Note: H.I, heat input; WoI, without inhibitor; PIE, percentage inhibitor efficiency; WI, with inhibitor; (), PIE for FCAW process; IAC, inhibitor accelerates corrosion

for WM and HAZ are shown in Table 9 and 10. Representative Tafel plots have been furnished in Fig. 12 and 13.

3.5 SEM Analysis

The WM region with four different heat inputs exposed to 0.5 M HCl containing 100 ppm hexamine was subjected to SEM examination, and the surface morphologies of corrosion film formed are shown in Fig. 14-17. In terms of surface morphology by SEM, detailed analyses have been reported by Mann (Ref 12) and others (Ref 13-16) pertaining to case studies. Similar observation has been made by Natarajan et al. in the case of Cr-Mo power plant low alloy steels for other welding processes (Ref 17-20). Magnetite film (Fe₃O₄) formation is the dominant effect of corrosion for the conditions used. Excessive thickening of the oxide can result in fissuring and exfoliation. In the micrograph shown for higher heat inputs, there is evidence of fissuring and pit formation which resembles with the figures reported by Mann at higher temperatures in respect of distributed chloride crystals coupled with grains

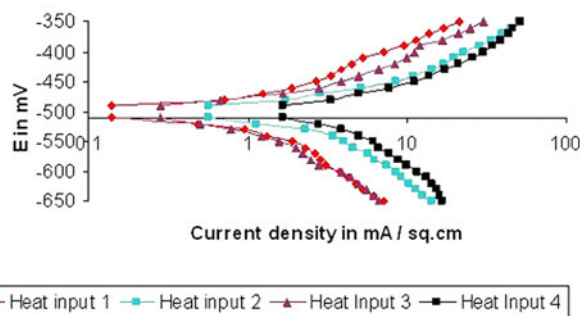


Fig. 12 Tafel graph/FCAW/2.25Cr-1Mo/WM/0.5 M HCl + hexamine/H.T

of (Fe₃O₄). Huybregts has also shown SEM micrographs that contain steam chimneys similar to those noted in this investigation.

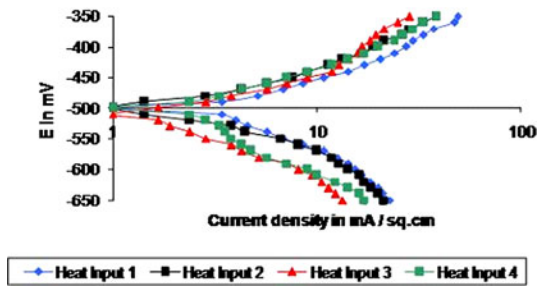


Fig. 13 Tafel graph/FCAW/2.25Cr-1Mo/WM/0.5 M HCl + mixed inhibitor/100 °C

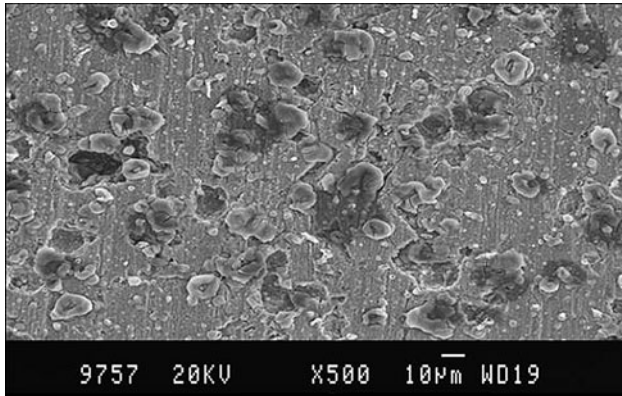


Fig. 14 SEM photograph of WM/2.25Cr-1Mo/FCAW with heat input 1 (1152 J/mm) showing spongy film with steam chimneys in between

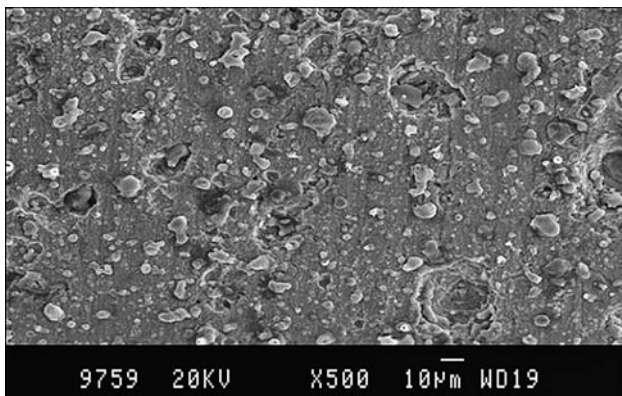


Fig. 15 SEM photograph of WM/2.25Cr-1Mo/FCAW with heat input 2 (1612 J/mm) shows oxide layer with pearls embedded on the surface

3.6 XRD Studies

The XRD pattern obtained on WM shows peaks that correspond to formation of Fe_2Si , FeSi_2 , γFeMn_3 , Fe_7Mo_3 , Fe_3O_4 , FeO , FeCr , $\text{AlO}_7\text{Fe}_3\text{SiO}_3$, and $\text{KFe}_4\text{Mn}_{77}\text{Si}_{19}$ as shown in Fig. 18. An indepth analysis of XRD by Kumaresh Babu et al. (Ref 21-25) on Cr-Mo steels as well as carbon steels for

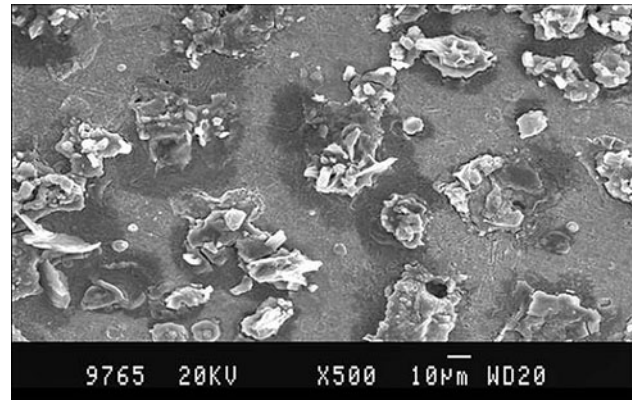


Fig. 16 SEM photograph of WM/2.25Cr-1Mo/FCAW with heat input 3 (2112 J/mm) continuous magnetite layer with apparent fissuring with steam chimneys

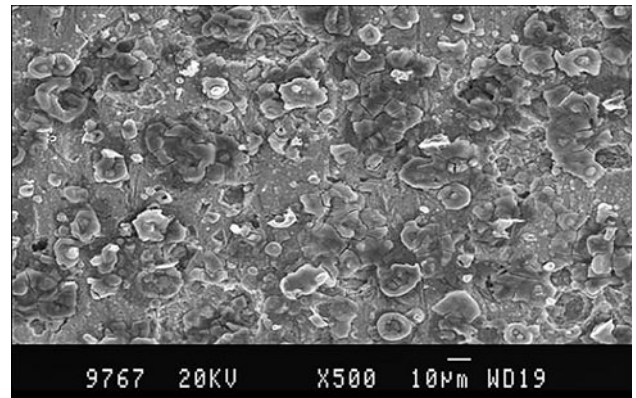


Fig. 17 SEM photograph of WM/2.25Cr-1Mo/FCAW with heat input 4 (2640 J/mm) resembles broken marble-like appearance with blisters

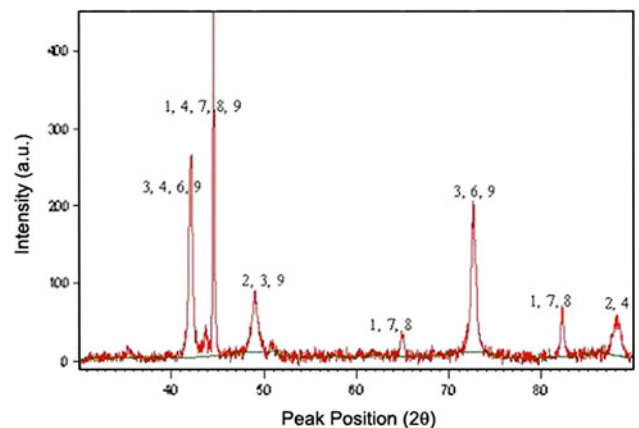


Fig. 18 XRD pattern of 2.25Cr-1Mo/FCAW/100 °C/WM/0.5 M HCl + 100 ppm hexamine. The peaks identified are: (1) FeSi ; (2) FeSi ; (3) FeMn ; (4) FeMo ; (5) FeO ; (6) FeO ; (7) FeCr ; (8) AlOFeSiO ; and (9) KFeMnSi

FCAW and other processes is worth mentioning at this juncture. It is to be pointed out that a series of compounds of different stoichiometry have been formed.

4. Conclusions

- As a result of increased heat input of the order of 1 kJ/mm in FCAW, a twofold increase in corrosion rate is observed in WM and HAZ regions.
- The inhibitor efficiency of mixed inhibitor is relatively better at 100 °C.
- SEM examination reveals spongy nature of film formation with micro fissures and steam chimneys.
- The XRD analysis indicates the formation of Fe₂Si, FeSi₂, γFeMn₃, Fe₇Mo₃, Fe₃O₄, FeO, FeCr, AlO₇Fe₃SiO₃, and KFe₄Mn₇₇Si₁₉.
- Experiments with fundamental approach adopted using different variables at 100 °C carried out on a laboratory scale lead to a better understanding of the corrosion phenomenon, and some of these observations resemble those of case studies made at still higher temperatures.

References

1. R.L.O. Brien, *Welding Hand Book*, 8th ed., AWS, 1995
2. Z. Zhang, A.W. Marshall, and G.B. Holloway, Advances in Materials Technology for Fossil Power Plants, *Proc. of 4th International Conference*, Vol 10, South Carolina, 2004, p 267–272
3. T.G. Gooch, The Effect of Welding on Corrosion, NACE Publication, *Process Industry Corrosion*, 1982, p 739–755
4. M. Henthorne, Corrosion Testing of Weldments, *Corrosion—NACE*, 1974, **30**(39)
5. G.E. Linnert, *Welding Metallurgy, Carbon and Alloy Steels*, 4 ed., Vol 1, AWS, Miami, Florida, USA, 1994
6. G.S. Theus and P.L. Daniel, Corrosion in Power Generating Equipment, *8th International Brown Boveri Symposium*, Baden, Switzerland, 1983, p 185–188
7. NACE, *Corrosion Testing of Chemical Cleaning Solvents*, Vol 21, NACE Publication 3M, 1982, p 48
8. V. Raghavan, *Physical Metallurgy*, Prentice-Hall of India, New Delhi, 1991
9. S.P. Kumaresh Babu and S. Natarajan, Corrosion Behaviour of Flux Cored Arc Welded 2.25Cr-1Mo Power Plant Steel with Different Heat Input—Fundamental Aspects (Part-I) (Communicated)
10. M.G. Fontana and R.W. Staehle, Ed., *Advances in Corrosion Science and Technology*, Vol 1, Plenum Press, p 190
11. S. Natarajan and V. Sivan, Impedance Measurements and High Temperature Weldment Corrosion in 2.25Cr-1Mo Steel Used in Power Plants, CORCON, *International NACE Conference Proc.*, Vol 11, Dec 1997 (Mumbai, India), Elsevier, 1997, p 652–661
12. G.M.W. Mann, History and Causes of On-Load Water Side Corrosion in Power Boilers, *Br. Corros. J.*, 1977, **12**(1), p 6–13
13. L. Kayafas, Corrosion Product Removal from Steel Fracture Surfaces for Metallographic Examination, *J. Corros.*, 1990, p 443
14. P. Mayer and A.V. Manolesu, Growth and Structure of Indigenous Magnetite on Boiler Tubes, *Proc. 7th ICMC*, Ontario, Canada, 1980, p 1480–1487
15. W.M.M. Huybregts, Protection Effectiveness of Magnetite Layers in Relation to Boiler Corrosion, *Proc. 5th ICMC*, Tokyo, Japan, 1972, p 857
16. P.H. Effertz, Morphology and Composition of Magnetite Layers in Boiler Tubes Following Long Exposure, *Proc. 5th ICMC*, Tokyo, Japan, 1972, p 920
17. S. Natarajan and V. Sivan, Influence of Induction Pressure Welding Process on Corrosion and Its Inhibition in SA 213 T11 (1Cr-0.5Mo) Low Alloy Steel Used in Power Plants, *Proc. of IIW National Welding Seminar*, Bangalore, India, Dec 1997, p 448–454
18. S. Natarajan, Corrosion Behaviour of GMA Weldments in 1Cr-0.5Mo Power Plant Steel, *Australas. Welding J.*, 2005, **50**, p 33–39 (II quarter)
19. S. Natarajan and V. Sivan, Weldment Corrosion and Its Inhibition in Power-Generating Components, *J. Corros. Prev. Control*, 2003, **50**(1), p 7–19
20. S. Natarajan and V. Sivan, High Temperature Corrosion and Its Inhibition in Carbon Steel Fusion Weldments Used in Power and Process Plants, *Int. J. Joining Mater. (JOM)*, 2003, **15**(3), p 17–24
21. S.P. Kumaresh Babu and S.Natarajan, Influence of Heat Input on Corrosion Behavior of Flux Cored Arc Weldments in 1Cr-0.5Mo Power Plant Steel (Communicated)
22. S.P. Kumaresh Babu and S.Natarajan, High Temperature Corrosion and Characterisation Studies in Flux Cored Arc Welded 1Cr-0.5Mo Power Plant Steel (Communicated)
23. S.P. Kumaresh Babu and S. Natarajan, Corrosion Behavior of Pulsed GTA Weldments in Power Plant Carbon Steel, *J. Mater. Eng. Perform.-ASM*, 2007, **16**(5), p 620
24. S.P. Kumaresh Babu and S. Natarajan, Influence of Heat Input on High Temperature Weldment Corrosion in Submerged Arc Welded Power Plant Carbon Steel, *J. Mater. Des. (Elsevier)*, 2008, **29**, p 1032–1042
25. S. Natarajan, S.P. Kumaresh Babu, and M. Ramesh, Corrosion Behavior of GTA Welded 9Cr-1Mo Power Plant Steel, *IWS Welding J.*, 2007, **3**, p 44–49